Biophysical Journal Volume 66 February 1994 394–401

Anomalous Diffusion Due to Obstacles: A Monte Carlo Study

Michael J. Saxton

Institute of Theoretical Dynamics, University of California, Davis, California 95616, and Laboratory of Chemical Biodynamics, Lawrence Berkeley Laboratory, University of California, Berkeley, California 94720 USA

ABSTRACT In normal lateral diffusion, the mean-square displacement of the diffusing species is proportional to time. But in disordered systems anomalous diffusion may occur, in which the mean-square displacement is proportional to some other power of time. In the presence of moderate concentrations of obstacles, diffusion is anomalous over short distances and normal over long distances. Monte Carlo calculations are used to characterize anomalous diffusion for obstacle concentrations between zero and the percolation threshold. As the obstacle concentration approaches the percolation threshold, diffusion becomes more anomalous over longer distances; the anomalous diffusion exponent and the crossover length both increase. The crossover length and time show whether anomalous diffusion can be observed in a given experiment.

INTRODUCTION

In unobstructed diffusion, the mean-square displacement of the diffusing particle is proportional to time. This follows directly from the solution to the classical diffusion equation. But in disordered systems diffusion may be anomalous: the mean-square displacement is proportional to a fractional power of time not equal to one. A variety of mechanisms lead to anomalous diffusion, involving broad distributions of jump times, broad distributions of jump lengths, or strong correlations in diffusive motion (Bouchaud and Georges, 1988; Bouchaud and Georges, 1990; Scher et al., 1991). For diffusion in cell membranes the relevant mechanisms are obstruction, which can produce strong correlations, and binding, which can produce a broad distribution of jump times. Diffusion is hindered, and the mean-square displacement is proportional to a fractional power of time less than one. Here we consider only obstruction; later work will treat binding.

Single-particle tracking experiments have provided evidence of anomalous diffusion of membrane proteins in cells (Ghosh and Webb, 1990; Ghosh, 1991). The low-density lipoprotein (LDL) receptor was labeled with a highly fluorescent form of LDL. Computer-enhanced video microscopy was used to track the trajectories of individual receptors as they moved on the cell surface. The time resolution was 1/30 s and the spatial resolution was 30 nm. The mean-square displacement was calculated by averaging within a single trajectory. In some trajectories, a log-log plot of the mean-square displacement as a function of time showed anomalous diffusion, and transitions between anomalous and normal diffusion were observed.

Anomalous diffusion may be observable in fluorescence photobleaching recovery experiments as well (Brust-Mascher et al., 1993). When anomalous diffusion occurs, the probability density for a diffusing particle is not the usual Gaussian distribution, but a stretched exponential (Klafter et al., 1992), so the form of the fluorescence recovery curve changes. Nagle (1992) has shown for one-dimensional systems that long-time tails in the jump rate of the diffusing species affect the shape of the photobleaching recovery curve. If such a recovery curve is analyzed by conventional means, the diffusion coefficient and the fractional recovery depend on the measurement time. Long-time tails may result from transient binding of the diffusing species to immobile species, if the distribution of binding energies is wide enough.

Anomalous diffusion has been studied in great detail in the percolation literature (reviewed in Havlin and Ben-Avraham, 1987; Bunde and Havlin, 1991; Havlin and Bunde, 1991; Stauffer and Aharony, 1992), but these results are restricted to obstacle concentrations at or near the percolation threshold. For biophysical applications, we need to consider a wider range of obstacle concentrations, from unobstructed diffusion to the percolation threshold. We shall examine the distance and time over which anomalous diffusion occurs and how large a deviation from normal diffusion occurs. The key quantity in the analysis is the ratio of the mean-square displacement $\langle r^2 \rangle$ to the time t. Earlier work (Saxton, 1989) examined this ratio as the distance-dependent diffusion coefficient $D^*(r)$.

The approximations in a lattice model of diffusion are summarized elsewhere (Scalettar and Abney, 1991; Saxton, 1993a). For purposes of this paper, the most important limitation of a lattice model is that it gives no information about dynamics on time scales less than the time required for a tracer to diffuse one lattice constant. For example, we neglect the decay of inertial terms, which takes place on a time scale of 10^{-13} s (Abney et al., 1989). Furthermore, hydrodynamic interactions are neglected, and small errors due to the discrete nature of the lattice may appear at distances less than a few lattice constants.

METHODS

Diffusion calculations are carried out as described earlier (Saxton, 1987; 1992). Obstacles are placed on the lattice at random at a prescribed con-

Received for publication 26 August 1993 and in final form 17 November 1993.

Address reprint requests to Michael J. Saxton at Institute of Theoretical Dynamics, University of California, Davis, CA 95616.

0006-3495/94/02/394/08 $2.00

centration. A tracer is placed at a random unblocked point on the lattice, and carries out a random walk on unobstructed lattice sites. Its position is recorded as a function of time, and the mean-square displacement $\langle r^2 \rangle$ is obtained by averaging the positions over different random walks with the same configuration of obstacles, and different configurations with the same area fraction of obstacles. Typically, 25 or 50 different obstacle configurations were used, and 200 or 400 random walks per obstacle configuration. In each run, 128K or 2048K time steps were used (1K = 1024). Calculations for fractal obstacles (Saxton, 1993a) and for mixtures of mobile and immobile obstacles (Saxton, 1990) were described earlier.

RESULTS

In normal diffusion, the mean-square displacement $\langle r^2 \rangle$ of a diffusing particle is given by

$$\langle r^2 \rangle = 4Dt, \tag{1}$$

where D is the diffusion coefficient, and t is time. In anomalous diffusion, we have instead

$$\langle r^2 \rangle \sim t^{2/d_w}, \tag{2}$$

where d_w is the anomalous diffusion exponent. If $d_w = 2$, we recover normal diffusion. For obstructed diffusion, $d_w > 2$, and diffusion is slowed down. Eq. 2 is obtained from theoretical arguments and is confirmed by Monte Carlo results (Havlin and Ben-Avraham, 1987; Havlin and Bunde, 1991). At obstacle concentrations below the percolation threshold, diffusion is anomalous at short distances and normal at long distances.

To convert the dimensionless units r^* and t^* used in the Monte Carlo calculations to experimental units r and t, we use the lattice constant ℓ as the unit of length, the jump time τ as the unit of time, and D_0 as the diffusion coefficient of the tracer in an unobstructed system. Then $r = \ell r^*$, $t = \tau t^*$, $D = D_0 D^*(C)$ with $D^*(0) = 1$, and

$$\ell^2 = 4D_0\tau. \tag{3}$$

Eq. 1 then yields $\langle r^{*2} \rangle = D^*(C)t^*$. In both sets of units, the obstacle concentration C is an area fraction, defined as the fraction of lattice points occupied by obstacles. We take ℓ to be (infinitesimally less than) the sum of the diameters of an obstacle and a tracer, so that a pair of adjacent obstacles will just block passage of a tracer between them. Then τ is the time required for a tracer to diffuse a mean-square distance of ℓ^2 in the unobstructed system, and the lattice model says nothing about dynamics on time scales faster than τ.

The form of Eq. 2 is awkward because the proportionality constant does not have dimensions of cm^2/s. Worse yet, d_w is a function of obstacle concentration so the dimensions of the proportionality constant vary with obstacle concentration. So it is convenient to rewrite Eq. 2 as

$$\langle r^2 \rangle = 4Dt(t/\tau)^{2/d_w - 1}, \tag{4}$$

which can be transformed similarly to $\langle r^* \rangle^2 = D^*(C)t^{*2/d_w}$. To simplify the notation, we drop the asterisks in r^* and t^*, except in the discussion of crossover times.

Anomalous diffusion

Anomalous diffusion has been analyzed using percolation theory (Havlin and Ben-Avraham, 1987; Bunde and Havlin, 1991; Havlin and Bunde, 1991; Stauffer and Aharony, 1992). At obstacle concentrations below the percolation threshold, there is a percolation cluster, that is, a cluster of unobstructed lattice sites that provides a continuous path for long-range diffusion. The percolation cluster is fractal over short distances, and homogeneous over long distances (Kapitulnik et al., 1983; Bunde and Havlin, 1991). If the fractal dimension is d_f, the mass within a radius r is

$$M(r) \sim \begin{cases} r^{d_f} & r \ll \xi \\ r^2 & r \gg \xi. \end{cases} \tag{5}$$

Here ξ is the correlation length, a measure of the average length of the holes in the percolation cluster. A similar crossover occurs in the mean-square displacement

$$\langle r^2 \rangle \sim \begin{cases} t^{2/d_w} & r \ll R^*_{CR} \\ t & r \gg R^*_{CR}, \end{cases} \tag{6}$$

where R^*_{CR} is the crossover length. The correlation length and the crossover length diverge as the obstacle concentration C approaches the percolation threshold C_P

$$\xi \sim |C - C_P|^{-\nu}, \tag{7}$$

$$R^*_{CR} \sim |C - C_P|^{-\nu+\beta/2}, \tag{8}$$

where $\nu = 4/3$ and $\beta = 5/36$ are two-dimensional scaling exponents. The exponent ν is defined by Eq. 7, and β gives the probability that a lattice site is part of the infinite cluster, $P(\infty) \sim |C - C_P|^{\beta}$. At the percolation threshold, $\xi \to \infty$, and the percolating cluster is self-similar over all length scales, with no characteristic length scale (as is well illustrated in Feder, 1988, Fig. 7.9.) Because the percolating cluster is self-similar at C_P, the diffusion coefficient at C_P is time-dependent for all times. As time increases, the diffusing particle encounters dead ends, bottlenecks, and other hindrances at longer and longer length scales. A particle may escape a small dead end only to find that it is still trapped in a larger dead end.

Plots of mean-square displacement

If the mean-square displacement is plotted as a function of time (Fig. 1 *a*), the curves appear to be linear. As the obstacle concentration increases, the slope decreases, yielding the usual decrease in D^* with C. No structure is apparent at this scale. At a thousandfold higher magnification (Fig. 1 *b*), the lines for high obstacle concentrations show a slight curvature. To test for anomalous diffusion, the data can be replotted as log $\langle r^2 \rangle$ versus log t (Fig. 1 *c*). Normal diffusion yields a slope of 1; anomalous diffusion, a slope of $2/d_w \leq 1$. A small change in slope with time can be seen for $C \geq 0.3$.

To obtain a clear picture of the time dependence, we remove the linear dependence and plot $\log[\langle r^2 \rangle / t]$ as a function of $\log t$ (Fig. 1 *d*). Then normal diffusion yields a line of slope

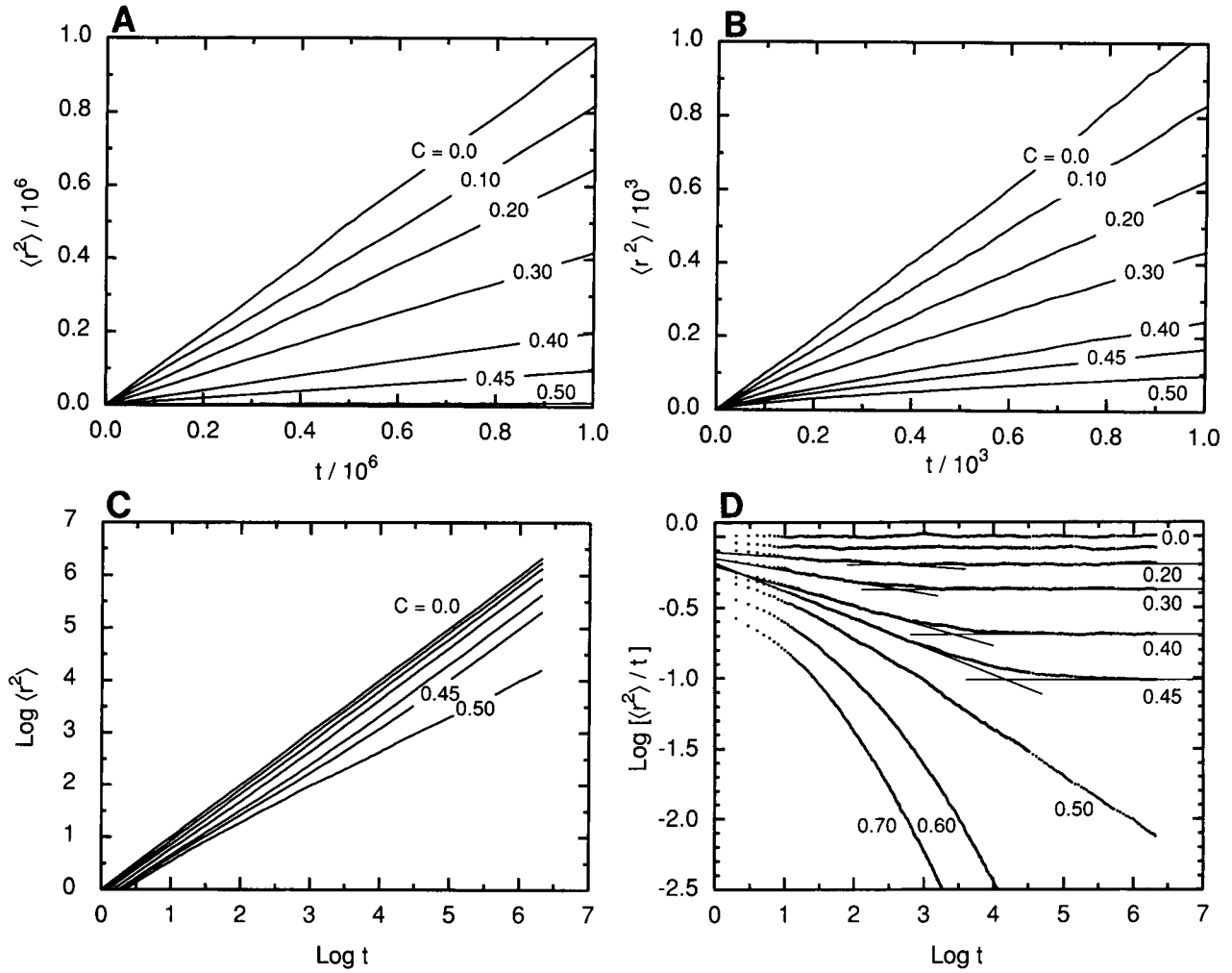

FIGURE 1 (*a*) Mean-square displacement $\langle r^2 \rangle$ as a function of time t for diffusion of a point tracer on a triangular lattice in the presence of point obstacles at the indicated obstacle concentrations C. Both $\langle r^2 \rangle$ and t are scaled by a factor of 10^6. Little structure is apparent. (*b*) The same data replotted at a thousandfold higher magnification. Here $\langle r^2 \rangle$ and t are scaled by a factor of 10^3, and a slight change in slope with time is evident for $C \geq 0.30$. (*c*) The same data replotted as log $\langle r^2 \rangle$ as a function of log t. Again, the slight change in slope with time is evident for $C \geq 0.30$. (*d*) The same data replotted as log $[\langle r^2 \rangle / t]$ as a function of log t.The method of data analysis is shown for several concentrations. The horizontal lines are the average value of log $[\langle r^2 \rangle / t]$ for large t. The slanted lines are least-squares fits of a straight line to the Monte Carlo results for small t. A few initial points are sometimes excluded from the least-squares fit. (Presumably the deviation for these points is due to the discrete nature of the lattice.) The intersection of the two lines defines the crossover time t^*_{CR}, and R^*_{CR} is obtained from Eq. 9. Also shown are results for $C = 0.60$ and 0.70, above the percolation threshold.

0, and anomalous diffusion yields a line of slope $2/d_w - 1$. At short times, diffusion is anomalous; at long times, diffusion is normal. The crossover from anomalous to normal diffusion occurs at a crossover time t^*_{CR}; the corresponding crossover distance is

$$R^*_{CR} = \sqrt{D^*(C, \infty) t^*_{CR}}, \qquad (9)$$

where $D^*(C, \infty)$ is the limiting value of $\langle r^{*2} \rangle / t^*$ for large t^*.

The anomalous diffusion exponent d_w, the crossover time t^*_{CR}, the crossover length R^*_{CR}, and the limiting value of the diffusion coefficient $D^*(C, \infty)$ are all functions of obstacle concentration. As the obstacle concentration increases, the crossover length increases. At the percolation threshold, ξ and R^*_{CR} become infinite (Eqs. 7, 8). The percolation cluster of unobstructed sites becomes a fractal on all length scales, and diffusion is anomalous over all distances (Fig. 1 *d*, $C = 0.5$). Above the percolation threshold (Fig. 1 *d*, $C = 0.6, 0.7$), diffusion is anomalous for short times; the limiting behavior for large times is discussed later.

The existence of a crossover time is not an artifact of the finite lattice size used in the Monte Carlo calculations. Fig. 2 shows plots of $\log[\langle r^2 \rangle / t]$ versus log t for several independent runs at the same obstacle concentration for different times and different lattice sizes. This figure shows the magnitude of the statistical error at moderate concentrations, and more importantly, it shows that runs for different lattice sizes yield the same crossover length.

Anomalous diffusion requires the presence of immobile obstacles. Fig. 3 shows the behavior of a mixture of mobile point tracers and immobile point obstacles as the proportion of mobile and immobile species is changed at fixed total concentration (Saxton, 1990). If all the particles are mobile, diffusion is approximately normal. As the concentration of mobile particles decreases, diffusion becomes more anoma-

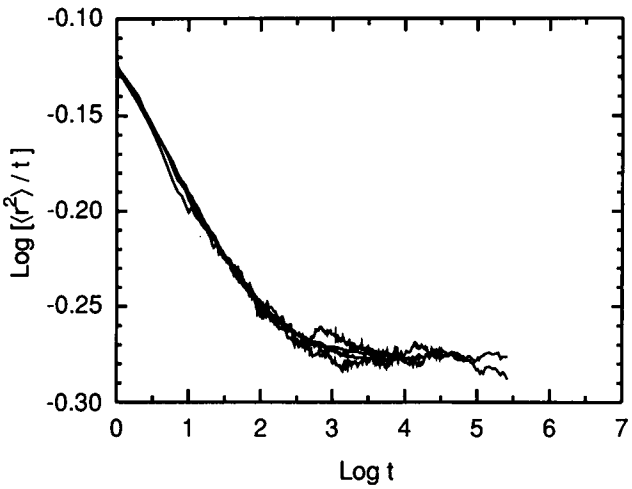

FIGURE 2 Log[$\langle r^2 \rangle / t$] as a function of log t for diffusion of a point tracer on a triangular lattice in the presence of point obstacles at $C = 0.25$.The vertical scale is expanded tenfold compared with Fig. 1 *d*. For a lattice size of 32 ×32, the run time was 4K (1K = 1024); for 64 ×64, 16K; for 128 ×128, 64K; and for 256 ×256, 256K. Another run used a 32 ×32 lattice and a 256K run time. As the run times were increased, fewer tracers were used, so the noise levels in the curves are different.

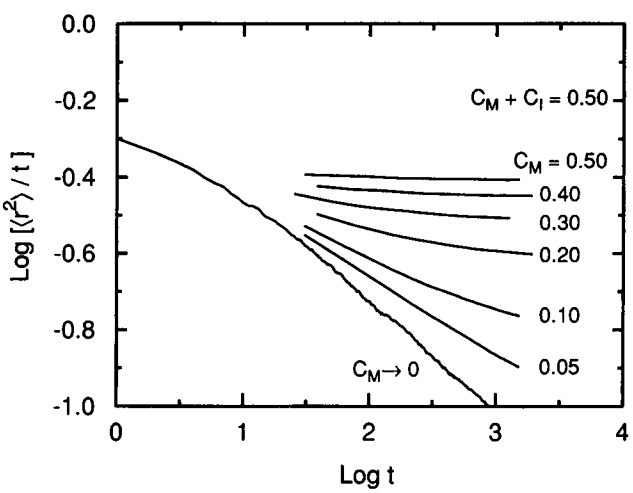

FIGURE 3 Log[$\langle r^2 \rangle / t$] as a function of log t for diffusion in a mixture of mobile point tracers (concentration C_M) and immobile point obstacles (concentration C_I) at a fixed total concentration $C_M + C_I = 0.5$ on the triangular lattice (Saxton, 1990). The percolation threshold is 0.5.

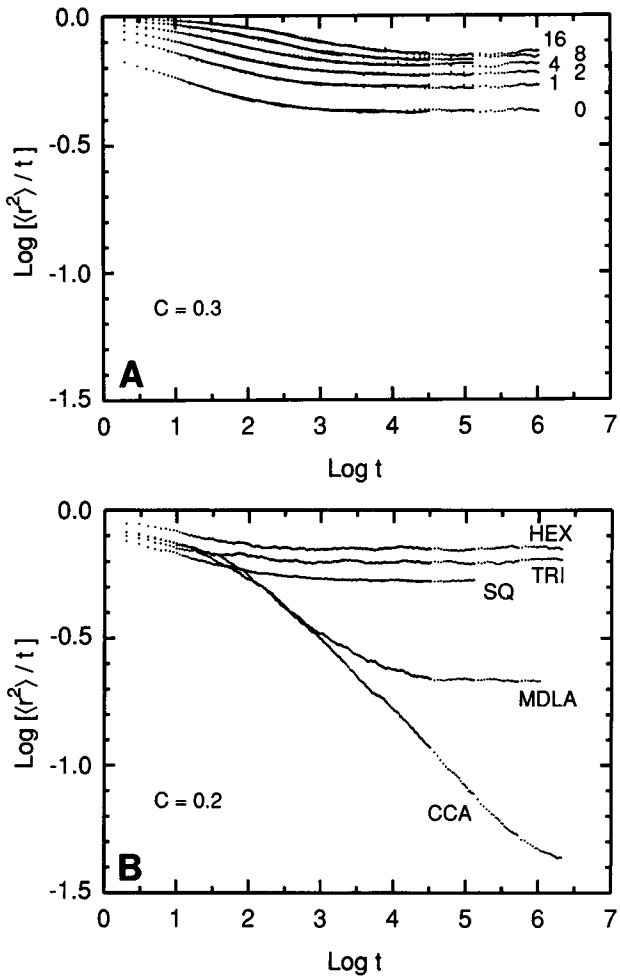

FIGURE 4 Variation of the curve of log[$\langle r^2 \rangle / t$] versus log t with obstacle geometry. (*a*) Monte Carlo results for point obstacles (radius 0) and hexagonal obstacles of radius 1, 2, 4, 8, and 16, at a fixed concentration $C = 0.3$, for a 512 ×512 grid. For each radius, six independent runs were made with different times and resolutions (Saxton, 1989); the scatter and irregularities are statistical noise. (*b*) Monte Carlo results for an obstacle concentration $C = 0.2$ for point obstacles on the square lattice (SQ); and point obstacles (TRI), hexagonal obstacles of radius 1 (HEX), multicenter diffusion-limited aggregates (MDLA), and cluster-cluster aggregates (CCA) on the triangular lattice.

lous. Abney et al. (1989) used a generalized Smoluchowski equation to examine the diffusion coefficient for mobile particles on the continuum; the diffusion coefficient reaches itssteady-state limit within one or two times the average interparticle distance. This result supports the use of a lattice model over longer distances.

At a given obstacle concentration, the shape of the curves of log[$\langle r^2 \rangle / t$] versus log t depends on the lattice and the type of obstacles. Fig. 4 *a* shows the curves for point obstacles and hexagonal obstacles of radius 1, 2, 4, 8, and 16 on the triangular lattice at a fixed obstacle concentration of $C = 0.3$. As the obstacle size increases, the correlation length and time increase, but the effect on $D^*(C, \infty)$ grows smaller and d_w approaches 2. Fig. 4 *b* shows the curves for an obstacle concentration $C = 0.2$ for point obstacles, hexagonal obstacles of radius 1, cluster-cluster aggregates, and multicenter diffusion-limited aggregates (Saxton, 1993a) on the triangular lattice, and point obstacles on the square lattice. Diffusion is much more anomalous in the presence of the two fractal aggregates. The size of a multicenter diffusion-limited aggregate for $C = 0.2$ is ~ 10, as measured by its pair correlation function (Saxton, 1993a), and its crossover time is similar to that of the larger hexagons. But anomalous diffusion is much more pronounced for the fractal obstacle than for the hexagonal obstacles.

The concentration dependence of d_w

The anomalous diffusion exponent measures the deviation from normal diffusion. Fig. 5 *a* shows d_w as a function of

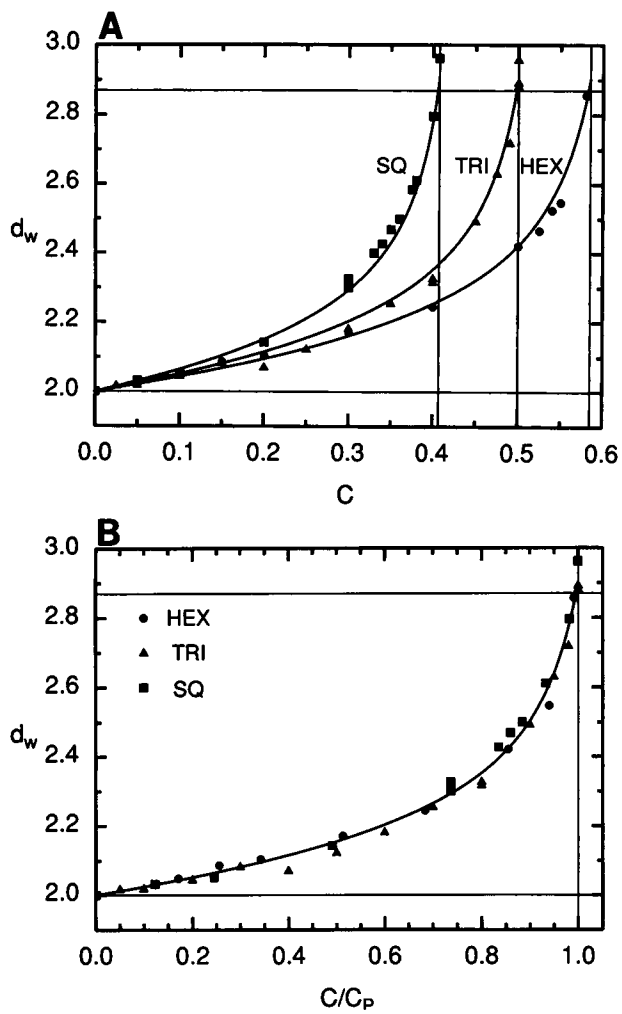

FIGURE 5 (*a*) Anomalous diffusion exponent d_w as a function of obstacle concentration C for three different geometries: point obstacles on the square lattice (SQ), point obstacles on the triangular lattice (TRI), and hexagonal obstacles of unit radius on the triangular lattice (HEX). The vertical lines show the percolation thresholds C_P, and the horizontal lines show the limiting values $d_w = 2$ for $C = 0$ and $d_w = 2.87$ for $C = C_P$. The smooth curves are from the expression for d_w in Fig. 5 *b*. (*b*) Anomalous diffusion exponent as a function of C/C_P. Values of the percolation threshold are 0.5000 for point obstacles on the triangular lattice (Stauffer and Aharony, 1992); 0.4073 for point obstacles on the square lattice (Stauffer and Aharony, 1992), and 0.5852 for hexagonal obstacles of unit radius on the triangular lattice (Saxton, 1993a). In the percolation literature, percolation thresholds are usually given in terms of the concentrations of unblocked sites, not the obstacle concentration. The smooth curve is a least-squares fit to the values of d_w: $d_w = (2 - 2.135\,x + 0.324\,x^2)/(1 - 1.184\,x + 0.249\,x^2)$, with $x = C/C_P$.

obstacle concentration for three different geometries: point obstacles on the square lattice, point obstacles on the triangular lattice, and hexagonal obstacles on the triangular lattice. The limiting values are known. At $C = 0$, diffusion is normal and $d_w = 2$; at the percolation threshold C_P, $d_w = 2.87$ for particles diffusing on the infinite cluster (Havlin and Bunde, 1991). Each curve goes to this limit at the appropriate percolation threshold. If the data are replotted as a function of C/C_P, they fall on the same curve, as shown in Fig. 5 *b*.

Near the percolation threshold, some diffusing particles are trapped in bounded regions; well above the percolation threshold, all the diffusing particles are trapped. The bounded regions grow smaller as the obstacle concentration increases. For trapped particles, as $t \to \infty$, $\langle r^2 \rangle$ approaches a constant value proportional to the average size of the bounded regions, so the slope of log $[\langle r^2 \rangle / t]$ versus log t approaches -1 (Fig. 1 *d*, $C = 0.6, 0.7$), and $d_w \to \infty$. This increase accounts for the fact that the exponent $d'_w = 2.95$ for diffusion on any cluster is greater than the exponent $d_w = 2.87$ for diffusion on the percolating cluster (Havlin and Bunde, 1991). This effect can be seen in Fig. 5 *a* for the triangular lattice at C_P. The highest point is for diffusion on all clusters, and the two lower points are for diffusion restricted to the percolating cluster.

A concentration-dependent exponent has been used to describe the number of distinct sites visited in an obstructed random walk (Argyrakis and Kopelman, 1984).

The concentration dependence of R^*_{CR} and t^*_{CR}

The crossover length R^*_{CR} and the crossover time t^*_{CR} describe the range of anomalous diffusion. They may be used to determine whether anomalous diffusion is observable for a given observation time and diffusion coefficient. Fig. 6 *a* shows log R^*_{CR} as a function of log $|C - C_P|$, the distance from the percolation threshold, and Fig. 6 *b* shows log t^*_{CR} versus log $|C - C_P|$. In both figures, the data points for different geometries fall roughly on the same curve, with the data points for hexagonal obstacles slightly higher than those for point obstacles.

Near the percolation threshold, R^*_{CR} and t^*_{CR} obey scaling laws (Havlin and Ben-Avraham, 1987; Bunde and Havlin, 1991; Havlin and Bunde, 1991; Stauffer and Aharony, 1992). Recall that from Eq. 8, $R^*_{CR} \sim |C - C_P|^{-\nu+\beta/2}$. Now $D \sim |C - C_P|^{\mu}$, with $\mu = 1.299$ for two-dimensional diffusion, so, from Eq. 9, $t^*_{CR} \sim |C - C_P|^{-z}$, with $z = \mu + 2\nu - \beta$. Far from the threshold, however, these scaling laws break down.

Unfortunately, near the threshold it is hard to get good values of R^*_{CR} and t^*_{CR} because t^*_{CR} is so large that very long computer runs are needed to see the crossover region. Far from the threshold, the crossover is easy to see, but the deviations from the scaling laws are significant. The results in Fig. 6 are nonetheless useful for estimating when anomalous diffusion and the crossover are observable.

The concentration dependence of $D^*(C, \infty)$

Finally, we consider the limiting value of the diffusion coefficient for large times, $D^*(C, \infty)$. Values of $D^*(C, \infty)$ are shown as a function of obstacle concentration C in Fig. 7 *a* for three different geometries. For consistency, $D^*(C, \infty)$ is obtained from the limiting values of $\langle r^2 \rangle / t$ at long times, as shown in Fig. 1 *d*, but a simple least-squares fit of a straight line to $\langle r^2 \rangle$ versus t (Fig. 1 *a*, *b*) gives values of $D^*(C, \infty)$ indistinguishable on the scale of Fig. 7. In the least-squares

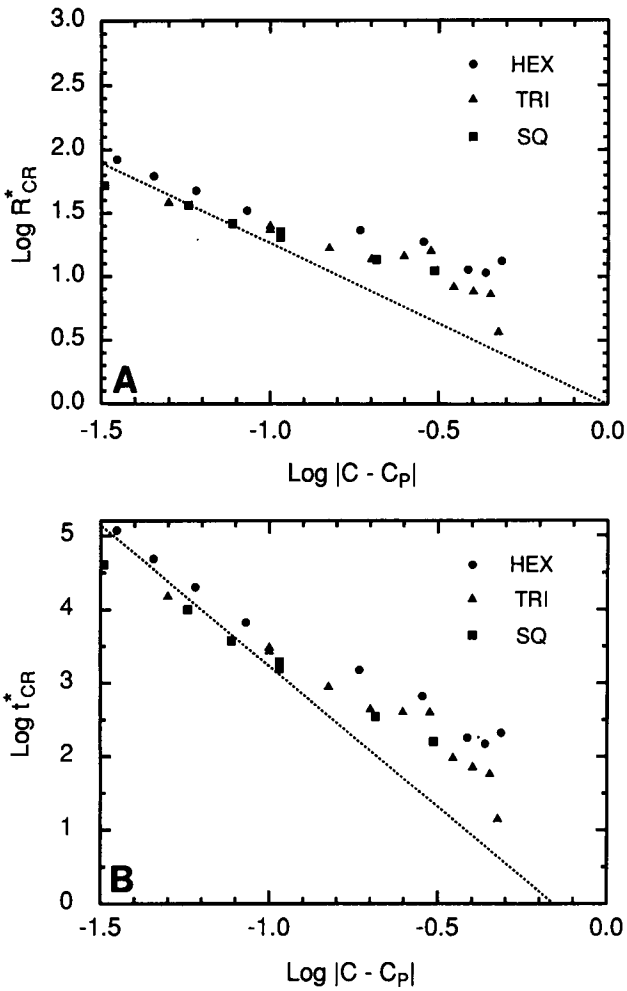

FIGURE 6 (*a*) Log-log plot of the crossover length R^*_{CR} as a function of the distance $|C - C_P|$ from the percolation threshold. (*Dotted line*) theoretical limiting slope $-\nu + \beta/2 = -1.2639$. (*b*) Log-log plot of the crossover time t^*_{CR} as a function of $|C - C_P|$. (*Dotted line*) theoretical limiting slope $-z = -3.8278$. Values of R^*_{CR} and t^*_{CR} were obtained from Monte Carlo calculations analyzed as in Fig. 1 *d*.

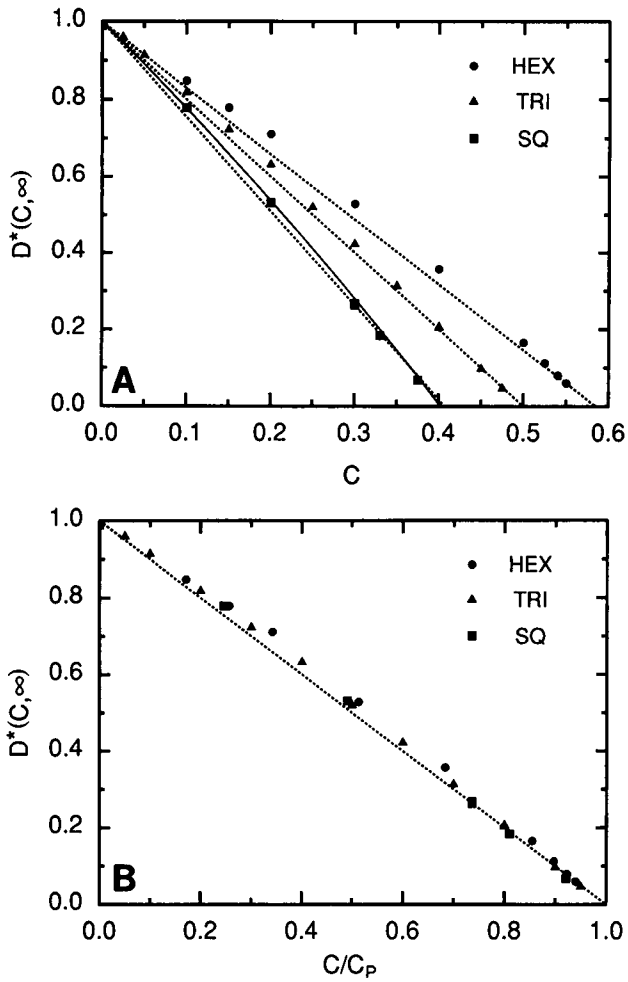

FIGURE 7 (*a*) Diffusion coefficients $D^*(C, \infty)$ as a function of obstacle concentration C for three different geometries: hexagonal obstacles of unit radius on the triangular lattice (HEX), point obstacles on the triangular lattice (TRI), and point obstacles on the square lattice (SQ). (*Dashed line*) $D^* = 1 - C/C_P$ for each geometry. (*Line*) theoretical expression for the diffusion coefficient for a square lattice (Nieuwenhuizen et al., 1986). (*b*) The same data replotted as a function of C/C_P. (*Dashed line*) $D^* = 1 - C/C_P$.

fit, the *y*-intercept is a free parameter. Also shown in Fig. 7 *a* are the lines $D^* = 1 - C/C_P$ for each geometry, and the theoretical expression of Nieuwenhuizen et al. (1986) for the diffusion coefficient for a square lattice, $D^* = 1 - (\pi - 1)C - 0.85571\,C^2$. If $D^*(C, \infty)$ is replotted as a function of C/C_P, the points fall approximately on a single curve (Fig. 7 *b*) close to the line $D^* = 1 - C/C_P$ but systematically higher except at the endpoints.

CONCLUSIONS

We have shown how anomalous diffusion can be characterized by the anomalous diffusion exponent d_w, the crossover length R^*_{CR} and time t^*_{CR}, and the limiting diffusion coefficient $D^*(C, \infty)$. As the concentration of obstacles increases to the percolation threshold, d_w varies smoothly between the known limiting values for normal diffusion and percolation. The parameters are approximately independent of the lattice when plotted as a function of the appropriate concentration variable.

When will experiments show anomalous diffusion in membranes? The most important consideration is the time scale. The time scale for fluorescence quenching and excimer formation is set by the fluorescence lifetime of the probe, typically in the nanosecond range. The time resolution for fluorescence photobleaching recovery is in the range of milliseconds or greater; for single-particle tracking the resolution is typically 33 ms.

Suppose that the obstacle is an immobile protein of diameter 4 nm. (If it is a cylinder of height 10 nm and density 1.3 g/cm^3, its mass is then $\simeq$ 100 kD.) In Eq. 3, the lattice constant ℓ is equal to the sum of the diameters of an obstacle and a tracer. If the tracer is a lipid of diameter 0.8 nm and diffusion coefficient 5 μm^2/s, then $\tau = 1.2$ μs, so quenching and excimer experiments will see only anomalous diffusion.

TABLE 1 Crossover times for anomalous diffusion of a 4-nm diameter tracer in the presence of 4-nm diameter obstacles at the indicated concentrations C

D_0 (cm^2/s)	τ	t_{CR} ($C = 0.30$)	t_{CR} ($C = 0.40$)	t_{CR} ($C = 0.45$)
10^{-8}	16 μs	6.4 ms	40 ms	400 ms
10^{-9}	160 μs	64 ms	400 ms	4 s
10^{-10}	1.6 ms	640 ms	4 s	40 s
10^{-11}	16 ms	6.4 s	40 s	400 s
10^{-12}	160 ms	64 s	400 s	4000 s

From Fig. 6 *b*, t^*_{CR} ranges from 10^2 to 10^5 depending on obstacle concentration, so the crossover time t_{CR} ranges from 120 μs to 120 ms. Photobleaching and tracking experiments will see only normal diffusion unless the system is very close to the percolation threshold.

For the same obstacles, suppose that the tracer is a mobile protein of diameter 4 nm, so that $\ell = 8$ nm. If D_0(protein) is estimated from D_0(lipid) using the Saffman-Delbrück equation (Saffman and Delbrück, 1975), then D_0(protein) $\simeq$ 0.75 D_0(lipid) (assuming a lipid viscosity of 1 poise, an aqueous viscosity of 0.01 poise, a bilayer thickness of 5 nm, a lipid radius of 0.4 nm, and a protein radius of 2 nm). Then τ = 4.3 μs and the behavior of protein and lipid tracers will be similar.

But if D_0(protein) is lowered further by factors other than obstruction (reviewed in Scalettar and Abney, 1991), anomalous diffusion may be observed in photobleaching and tracking experiments. These factors include hydrodynamic interactions (Bussell et al., 1992), and perturbation of lipids by obstacles (Almeida et al., 1992). Transient binding of the tracer to immobile species (Zhang et al., 1993) may also lower the diffusion coefficient; this case will be discussed in detail elsewhere.

Table 1 shows crossover times for 4-nm diameter tracers in the presence of 4-nm diameter obstacles for various obstacle concentrations and values of D_0. Here the values of the dimensionless crossover time t^*_{CR} were obtained from Fig. 6 *b*. If D_0 is low enough, and the obstacle concentration is close enough to the percolation threshold, anomalous diffusion and the crossover to normal diffusion can be seen in single-particle tracking experiments with the usual sampling time of 33 ms, and will affect the recovery curve in photobleaching experiments. But if the obstacle concentration is low, the measurements will show only normal diffusion. At low obstacle concentrations the anomaly is small enough (Fig. 1 *d*) that it can easily be lost in experimental noise anyway.

In deciding whether anomalous diffusion can be seen in tracking experiments, we must also consider averaging. In these experiments, statistical fluctuations are significant, and data analysis must take the randomness of an observed trajectory into account (Saxton, 1993b). The noise can be reduced by averaging over a large number of independent trajectories, as is done in the Monte Carlo calculations. One can also average within a single trajectory, as discussed by Ghosh (1991) and by Qian et al. (1991). (For example, the mean-square displacement for $t = 2$ is taken to be the average over all displacements, or all independent displacements, two time steps apart.) This may make it possible to extract a sufficiently smooth mean-square displacement from a single trajectory to see anomalous diffusion.

For concentrations of obstacles near the percolation threshold, anomalous diffusion and the crossover to normal diffusion may be observable in single-particle tracking experiments if the diffusion coefficient in the unobstructed system is below $\simeq 10^{-10}$ cm^2/s. For slow protein diffusion, the problem in seeing anomalous diffusion is not the time scale of the experiment, but being able to do enough averaging. If enough averaging can be done, plots of $\log[\langle r^2\rangle/t]$ versus $\log t$ may be a useful means of data analysis.

At moderate and high obstacle concentrations, measurements of fluorescence quenching and excimer formation are likely to show only anomalous diffusion. Near the percolation threshold, the effects of a fractal substrate on reaction rates (Kopelman, 1988) should be considered.

I thank Paulo Almeida, Mary Blackwell, Lan Huang, John Nagle, and Matt Petersheim for helpful discussions; Paulo Almeida, Mary Blackwell, and a reviewer for comments on the manuscript; and Ken Jacobson for a preprint of his paper. This work was supported by National Institutes of Health grant GM38133.

REFERENCES

Abney, J. R., B. A. Scalettar, and J. C. Owicki. 1989. Self diffusion of interacting membrane proteins. *Biophys. J.* 55:817–833.

Almeida, P. F. F., W. L. C. Vaz, and T. E. Thompson. 1992. Lateral diffusion and percolation in two-phase, two-component lipid bilayers. Topology of the solid-phase domains in-plane and across the lipid bilayer. *Biochemistry.* 31:7198–7210.

Argyrakis, P., and R. Kopelman. 1984. Fractal to Euclidean crossover and scaling for random walkers on percolation clusters. *J. Chem. Phys.* 81: 1015–1018.

Bouchaud, J.-P., and A. Georges. 1988. The physical mechanisms of anomalous diffusion. In E. Guyon, J.-P. Nadal, and Y. Pomeau, eds., Disorder and Mixing (Kluwer Academic Publishers, Dordrecht) 19–29.

Bouchaud, J.-P., and A. Georges. 1990. Anomalous diffusion in disordered media: statistical mechanisms, models, and physical applications. *Phys. Reports* 195:127–193.

Brust-Mascher, I., T. J. Feder, J. P. Slattery, B. Baird, and W. W. Webb. 1993. FPR data on mobility of cell surface proteins reevaluated in terms of temporally constrained molecular motions. *Biophys. J.* 64:A354 (abstract).

Bunde, A., and S. Havlin. 1991. Percolation I. In A. Bunde and S. Havlin, eds., Fractals and Disordered Systems. Springer-Verlag, Berlin. 50–95.

Bussell, S. J., D. L. Koch, and D. A. Hammer. 1992. Hydrodynamic interactions between proteins in biological membranes. *Biophys. J.* 61:A291 (abstract).

Feder, J. 1988. Fractals. Plenum Press, New York. 116.

Ghosh, R. N. 1991. Mobility and clustering of individual low-density lipoprotein receptor molecules on the surface of human skin fibroblasts. Ph.D. thesis, Cornell University. 260 pp.

Ghosh, R. N., and W. W. Webb. 1990. Evidence for intra-membrane constraints to cell surface LDL receptor motion. *Biophys. J.* 57:286a (abstract).

Havlin, S., and D. Ben-Avraham. 1987. Diffusion in disordered media. *Adv. Phys.* 36:695–798.

Havlin, S., and A. Bunde. 1991. Percolation II. In A. Bunde and S. Havlin, eds., Fractals and Disordered Systems. Springer-Verlag, Berlin. 96–149.

Kapitulnik, A., A. Aharony, G. Deutscher, and D. Stauffer. 1983. Self similarity and correlations in percolation. *J. Phys. A* 16:L269–L274.

Klafter, J., M. F. Shlesinger, G. Zumofen, and A. Blumen. 1992. Scale invariance in anomalous diffusion. *Phil. Mag. B* 65:755–765.

Kopelman, R. 1988. Fractal reaction kinetics. *Science* 241:1620–1626.

Nagle, J. F. 1992. Long-tail kinetics in biophysics? *Biophys. J.* 63:366–370.

Nieuwenhuizen, T. M., P. F. J. van Velthoven, and M. H. Ernst. 1986. Diffusion and long-time tails in a two-dimensional site-percolation model. *Phys. Rev. Lett.* 57:2477–2480.

Qian, H., M. P. Sheetz, and E. L. Elson. 1991. Single particle tracking. Analysis of diffusion and flow in two-dimensional systems. *Biophys. J.* 60:910–921.

Saffman, P. G., and M. Delbrück. 1975. Brownian motion in biological membranes. *Proc. Natl. Acad. Sci. USA* 72:3111–3113.

Saxton, M. J. 1987. Lateral diffusion in an archipelago: the effect of mobile obstacles. *Biophys. J.* 52:989–997.

Saxton, M. J. 1989. Lateral diffusion in an archipelago: distance dependence of the diffusion coefficient. *Biophys. J.* 56:615–622.

Saxton, M. J. 1990. Lateral diffusion in a mixture of mobile and immobile particles: a Monte Carlo study. *Biophys. J.* 58:1303–1306.

Saxton, M. J. 1992. Lateral diffusion and aggregation: a Monte Carlo study. *Biophys. J.* 61:119–128.

Saxton, M. J. 1993a. Lateral diffusion in an archipelago: dependence on tracer size. *Biophys. J.* 64:1053–1062.

Saxton, M. J. 1993b. Lateral diffusion in an archipelago: single-particle diffusion. *Biophys. J.* 64:1766–1780.

Scalettar, B. A., and J. R. Abney. 1991. Molecular crowding and protein diffusion in biological membranes. *Comments Mol. Cell. Biophys.* 7: 79–107.

Scher, H., M. F. Shlesinger, and J. T. Bendler. 1991. Time-scale invariance in transport and relaxation. *Physics Today* 44 (no. 1):26–34.

Stauffer, D., and A. Aharony. 1992. Introduction to Percolation Theory. 2nd edition. Taylor and Francis, London. 181 pp.

Zhang, F., G. M. Lee, and K. Jacobson. 1993. Protein lateral mobility as a reflection of membrane microstructure. *BioEssays* 15:579–588.